Metabolomic profiles of cartilage and bone reflect tissue type, radiography-confirmed osteoarthritis, and spatial location within the joint

Hope D. Welhaven, Ethan Viles, Jenna Starke, Cameron Wallace, Brian Bothner, Ronald K. June, Alyssa K. Hahn.

Metabolomic profiles of cartilage and bone reflect tissue type, radiography-confirmed osteoarthritis, and spatial location within the joint

Hope D. Welhaven[a], Ethan Viles[b], Jenna Starke[c], Cameron Wallace[d], Brian Bothner[a], Ronald K. June[b], Alyssa K. Hahn[e]

[a]Department of Chemistry & Biochemistry, Montana State University, Bozeman, MT 59717, United States

[b]Department of Mechanical & Industrial Engineering, Montana State University, Bozeman, MT, 59717, United States

[c]Montana WWAMI, University of Washington School of Medicine, Seattle, WA, 98195, United States

[d]Department of Orthopaedic Surgery, University of Utah Health, Salt Lake City, UT 84103, United States

[e]Department of Biological and Environmental Sciences, Carroll College, Helena, MT, 59625, United States

Corresponding Author
Alyssa K. Hahn, PhD
Dept. of Biological and Environmental Sciences
Carroll College
1601 N Benton Ave, Helena, MT, 59625
Phone: 406-447-4370
E-mail: akhahn@carroll.edu
ORCID: 0000-0002-8884-2610

Author information:
Hope D. Welhaven: hopewelhaven@msu.montana.edu, ORCID: 0000-0001-9330-6903
Ethan Viles: ethan.viles@montana.edu, ORCID: 0000-0002-2854-5569
Jenna Starke: jennamstarke@gmail.com, ORCID: 0000-0002-1084-8537
Cameron Wallace: c33wallace@gmail.com, ORCID: 0000-0002-6462-327X
Brian Bothner: bbothner@montana.edu, ORCID: 0000-0003-1295-9609
Ronald K. June: rjune@montana.edu, ORCID: 0000-0003-0752-4109

HIGHLIGHTS

- Grades III and IV cartilage and bone exhibit distinct metabolic perturbations
- Metabolic alterations across the joint during late-stage disease are not uniform
- GAG homeostasis in each tissue is negatively influenced during late-stage OA
- Metabolic perturbations in tissue and space reveal OA crosstalk

ABSTRACT

Osteoarthritis is the most common chronic joint disease, characterized by the abnormal remodeling of joint tissues including articular cartilage and subchondral bone. However, there are currently no therapeutic drug targets to slow the progression of disease because disease pathogenesis is largely unknown. Thus, the goals of this study were to identify metabolic differences between articular cartilage and subchondral bone, compare the metabolic shifts in osteoarthritic grade III and IV tissues, and spatially map metabolic shifts across regions of osteoarthritic hip joints. Articular cartilage and subchondral bone from 9 human femoral heads were obtained after total joint arthroplasty, homogenized and metabolites were extracted for liquid chromatography-mass spectrometry analysis. Metabolomic profiling revealed that distinct metabolic endotypes exist between osteoarthritic tissues, late-stage grades, and regions of the diseased joint. The pathways that contributed the most to these differences between tissues were associated with lipid and amino acid metabolism. Differences between grades were associated with nucleotide, lipid, and sugar metabolism. Specific metabolic pathways such as glycosaminoglycan degradation and amino acid metabolism, were spatially constrained to more superior regions of the femoral head. These results suggest that radiography-confirmed grades III and IV osteoarthritis are associated with distinct global metabolic and that metabolic shifts are not uniform across the joint. The results of this study enhance our understanding of osteoarthritis pathogenesis and may lead to potential drug targets to slow, halt, or reverse tissue damage in late stages of osteoarthritis.

Keywords: osteoarthritis, articular cartilage, bone, hip, metabolism

1. INTRODUCTION

Osteoarthritis (OA) is the most prevalent joint disease affecting over 32.5 million US adults, costs the US $185 billion per year, and is the leading cause of disability worldwide [1-4]. The current paradigm of OA pathogenesis suggests that disease results from metabolic imbalances at the tissue level where catabolic pathways outweigh anabolic pathways, resulting in abnormal remodeling and eventual breakdown of the articular cartilage (AC), subchondral bone (SB), and other surrounding tissues (e.g., synovitis) [5-7]. Although it is well established that metabolic dysfunction is associated with OA, global metabolomic profiling is advantageous because it detects thousands of small-molecule intermediates called metabolites to generate a global biochemical endotype that is representative of the overall physiological status of the tissue [8]. Applying this method to study AC and SB, additional insight into the role of metabolism in OA pathogenesis can be gained. A single study has utilized metabolomic profiling to analyze osteophyte cartilage tissue compared to cartilage from the lateral posterior femoral condyle, which exhibits similarities to healthy cartilage, and found that metabolic pathways altered were suggestive of cartilage degradation (phenylalanine, arginine, and proline metabolism) and endochondral ossification (taurine and hypotaurine metabolism)[9]. Similarly, only one previous study has employed metabolomic profiling of OA sclerotic SB compared to non-sclerotic SB and found that metabolic pathways altered were suggestive of a high rate of bone turnover and matrix deposition (taurine and hypotaurine metabolism, amino acid metabolism, pyrimidine and purine

metabolism) and regulation of inflammation and repair in damaged joints (sphingolipid metabolism). Despite these recent advances, more data are needed to clarify the metabolic derangement in joint tissues[10].

It is well-known that OA is a whole-joint disease, with established interdependence and crosstalk between AC and SB. Despite this, no study to date has investigated metabolic shifts in diseased AC and SB in a single study. This tissue-centric approach is limiting because it fails to investigate the potential crosstalk between AC and SB in disease progression. Therefore, the primary goal of this pilot study was to investigate the altered metabolism in OA tissues (AC and SB) that compose the osteochondral unit (OU) to gain a greater understanding of aberrant metabolism in disease progression. To accomplish this, metabolites were extracted from grades III and IV OA tissues (AC and SB) and analyzed by liquid chromatography-mass spectrometry-based global metabolomic profiling to gain insight into tissue-specific metabolic differences, the OU, and metabolic differences associated with grade in late-stage OA.

A secondary goal of this study was to spatially map metabolic shifts across the OA joint tissues to determine if metabolic dysfunction is uniform across the joint or locally constrained. Multiple studies have employed finite element models to spatially mapped the femoral head and found that load distribution is not uniform across the joint, showing that superior regions of the femoral head experience the greatest stress and cartilage contact pressure[11-14]. Furthermore, microscopic and macroscopic indicators of OA (e.g., chondrocyte clustering, AC lesions) are not uniformly distributed across diseased joint tissues[15,16]. Therefore, we hypothesized that metabolic alterations would not be uniform across the diseased joint and that regions that experience the greatest mechanical stress may exhibit greater evidence of OA metabolic perturbations. The identification of disease-associated metabolic shifts that localize to specific regions of the joint will provide insight into late-stage disease progression and may reveal new therapeutic targets for more spatially targeted treatments in the joint.

2. METHODS

2.1 Patients and femoral head samples

Under Institutional Review Board (IRB) approval, femoral heads from end-stage OA (grade III or IV) joints were obtained with consent following total joint arthroplasty. OA grade was assigned based on the widely accepted Kellgren-Lawrence grading scheme which scores radiographic characteristics on a scale of 0-4 with scores increasing with progression of OA. Radiographic characteristics that are considered evidence of OA include: osteophyte formation, sclerosis of SB, presence or absence of bony formations, and joint space narrowing which is a surrogate for AC thickness and meniscal integrity[17,18].

To investigate the relationship between spatial distribution of OU components and metabolism, femoral heads were separated into four quadrants for tissue collection. Quadrants were determined based on previous studies that have spatially mapped stress distributions across the femoral head (Fig. 1A-C)[11-14]. Femoral heads from end-stage OA joints exhibit substantial degradation, in particular in load-bearing regions. Therefore, it was not possible to obtain sufficient tissue from every quadrant for each femoral head. Femoral heads that did not have sufficient tissue collected from 6 out of the 8 quadrants (for both AC and SB) were excluded from this study. Therefore, while 18 femoral heads were initially obtained following total joint arthroplasty, 9 femoral heads had sufficient tissue in the required number of quadrants to be included in this pilot study (n=3 grade III, n=6 grade IV, n=9 excluded). Partial participant information was provided with each donated femoral head including age, sex, height, and weight (Table 1).

[insert Table 1]

2.2 Metabolite extraction and global metabolomic profiling via LC-MS

100 mg of AC (n=31) and 100 mg of underlying SB (n=34) were shaved from each quadrant using the established quadrant system (Fig. 1A-C). All AC shavings and SB punches were submerged in 1 mL of 3:1 methanol:water (Sigma Aldrich, St. Louis, MO) because methanol is miscible with water allowing efficient extraction of lipophilic and hydrophilic metabolites. Moreover, it can be easily removed via vacuum concentration as it is highly volatile. Next, all samples were and homogenized using a tissue grinder (SPEX SamplePrep, Metuchen, NJ) for 15 second increments until fully homogenized. Samples were centrifuged at 500 *x g* for 10 minutes to remove cells and debris. The supernatant was collected and 100 μL of 4:1 methanol:water was added to extract metabolites for 30 minutes at -20°C prior to centrifugation at 16100 *x g* for 5 minutes. A vacuum concentrator (Savant AES 1010, ThermoFisher Scientific, Waltham, MA) was used to evaporate solvent from the supernatant, and the dried pellet was resuspended with 500 μL of 1:1 acetonitrile:water (Sigma Aldrich, St. Louis, MO) for 30 minutes at -20°C prior to centrifugation at 16100 *x g* for 5 minutes. Solvent was evaporated from supernatant by vacuum concentration and the dried pellet was resuspended with 1:1 water:acetonitrile for liquid chromatography-mass spectrometry (LC-MS) analysis.

Following metabolite extraction, all samples were analyzed by liquid chromatography-mass spectrometry (LC-MS) analysis. Specifically, extracts containing lipid- and water-soluble metabolites were analyzed in positive mode using an Agilent 1290 UPLC system coupled to an Agilent 6538 Q-TOF mass spectrometer (Agilent, Santa Clara, CA). Separation of metabolites was achieved using a Cogent Diamond Hydride HILIC column (150 x 2.1 mm) (MicroSolv, Eatontown, NJ) and optimized gradient elution method to separate and elute polar metabolites including polar lipids. Spectra were consequently processed and analyzed as previously described[19-21].

[insert Figure 1]

2.3 Statistical and pathway analyses

Obtained MS1 data consisting of mass-to-charge ratios (m/z), metabolite abundances, and retention times were processed using Agilent Masshunter Qualitative Analysis software and MS Convert. All data were then exported and converted using XCMS. Next, data were log transformed to correct for non-normal distribution and autoscaled (mean centered and divided by standard deviation of each variable). All statistical analyses were conducted in MetaboAnalyst [22]. To visualize and analyze differences between groups, statistical analyses employed included unsupervised multivariate hierarchical cluster analysis (HCA) and principal component analysis (PCA), supervised partial least-squares discriminant analysis (PLS-DA), and univariate fold change analysis. Volcano plot analysis, which combines both fold change and statistical significance, was also performed. Here, false discovery rate (FDR) corrections using the Benjamini-Hochberg method were applied to correct for multiple comparisons and a metabolite features significance threshold of 0.05 was used. HCA was visualized as a heatmap to identify populations of co-regulated metabolites. Populations of differentially expressed metabolite features were mapped to metabolic pathways using pathway enrichment analyses using the Functional Analysis module in MetaboAnalyst. Pathway library Kyoto Encyclopedia of Genes and Genomes (KEGG) was used to match metabolite features to putative metabolite identifications

(mass tolerance: 5 ppm, positive mode). Pathway significance was determined using an FDR-corrected *a prior* threshold of $p < 0.05$.

3. RESULTS

3.1 Osteochondral unit components are metabolically distinct

In total, 1,570 metabolite features were detected by LC-MS in both diseased AC (n=31) and SB (n=34) collected from grade III and IV OA patients. To investigate if the metabolome of OU components were metabolically distinct, unsupervised (HCA, PCA) and supervised (PLS-DA) multivariate statistical analyses were performed (Fig. 2 A-C). HCA displayed nearly perfect clustering between AC and SB samples (Fig. 2A) and PCA showed minimal overlap between the profiles of each tissue. (Fig. 2B). Similarly, PLS-DA showed distinct separation between AC and SB (Fig. 2C). To further visualize OU metabolic endotypes and identify unique populations of statistically significant metabolite features, fold change and volcano plot analyses were performed. Fold change analysis identified 360 metabolite features that had higher concentrations in AC compared to SB, whereas 384 metabolite features had higher concentrations in SB compared to AC (Fig. 2D, Table S1). Furthermore, volcano plot analysis considers significance (FDR-corrected p-value < 0.05) and revealed that 318 metabolite features were significant and expressed in higher concentrations in AC compared to SB, and 372 metabolite features were significant and expressed in higher concentrations in SB compared to AC (Fig. 2E).

Next, statistically significant metabolite features identified by fold change and volcano plot analyses underwent pathway enrichment analysis. Metabolite features that had the highest concentration in AC, compared to SB, were involved in ubiquinone biosynthesis, porphyrin metabolism, and lipid metabolism (arachidonic acid metabolism, glycosphingolipid metabolism) (Table 2, Table S2). Conversely, metabolite features involved in amino acid metabolism (alanine, aspartate, glutamate, valine, leucine, isoleucine), nucleotide metabolism (pyrimidine metabolism, aminoacyl-tRNA biosynthesis), and energy metabolism (TCA cycle) were highest in concentration in SB compared to AC (Table 2, Table S2).

[insert Figure 2]
[insert Table 2]

3.2 Changes in metabolic profiles correspond to radiography-confirmed grade of OA

To examine if metabolic differences exist between grade III and IV OA OU tissues, a four-group comparison (grade III AC, grade IV AC, grade III SB, grade IV SB) was performed. HCA showed clustering of tissues within their respective cohorts (Fig. 3A). Specifically, both grades of AC cluster together as well as both grades of SB with near perfect separation within grade (Fig. 3A). PCA was then used to analyze the variation amongst the four groups and visualize their metabolomes. Clear separation was observed between tissues and tissue grade, with minimal overlap observed between cohorts (Fig. 3B). PLS-DA was used to further examine the four groups, with some overlap observed between cohorts (Fig. 3C).

Finally, a median intensity heatmap analysis was performed to visualize overall global metabolomic profiles to reveal patterns of co-regulated and differentially expressed metabolite features. Using ward clustering, clusters of metabolite features were identified and then subjected to pathway enrichment analyses where metabolites features were mapped to metabolic pathways (Fig. 3D). Metabolite features that had higher concentration in grade III AC mapped to the pentose phosphate pathway and lysine degradation (Fig. 3D, Cluster 2, Table 3, Table S3). Conversely, metabolite features higher in grade IV AC mapped to glycosaminoglycan (GAG) degradation,

biosynthesis of unsaturated fatty acids, and ubiquinone biosynthesis (Fig. 3D, Cluster 1, Table 3, Table S3). Metabolite features that were higher in concentration in grade III SB mapped to amino acid metabolism (valine, leucine, isoleucine, alanine, aspartate, glutamate), the TCA cycle, and pantothenate and CoA biosynthesis (Fig. 3D, Cluster 3, Table 3, Table S3). Finally, metabolite features that were higher in grade IV SB mapped to porphyrin metabolism, primary bile acid biosynthesis, and GAG degradation (Fig. 3D, Cluster 4, Table 3, Table S3). Therefore, a shared pathway between grade IV tissues, both AC and SB, was GAG degradation.

[insert Figure 3]

Pairwise comparisons were also performed to investigate the metabolomes of samples that differ by tissue (grade III AC vs. grade III SB; grade IV AC vs. grade IV SB) and OA grade (AC grade III vs grade IV; SB grade III vs. grade IV). Pairwise comparisons revealed distinct metabolomes between tissues and OA grade (Fig. 4-5; Fig. S1-2; Table 3, Tables S4-7). The results of pairwise comparisons are further discussed in the Supplemental Material. Overall, the results of pathway enrichment analyses of fold change, volcano plot, and median metabolite intensity heatmaps from pairwise and multigroup comparisons strongly suggest that the metabolic endotypes of OU components reflect OA grade (Table 3).

[insert Figure 4]
[insert Figure 5]
[insert Table 3]

3.3 Metabolic endotypes differ based on spatial location

Lastly, AC and SB from late-stage OA participants that differ by spatial location were examined using a four-quadrant system (Fig. 1A-C). Specifically, quadrants 1 and 2 corresponded to anterior superior and inferior regions, whereas quadrants 3 and 4 corresponded to posterior superior and inferior regions, respectively. To investigate the metabolome of AC and SB quadrants, HCA and PLS-DA were used to visualize data. Both statistical tests displayed overlap between AC (Fig. 6A-B) and SB (Fig. 6D-E) quadrants which can be attributed to quadrants clustering by patient.
[insert Figure 6]

To identify clusters of co-regulated and differentially expressed metabolite features in AC quadrants, a median intensity heatmap analysis was performed. Clusters then underwent pathway enrichment analyses to identify biological pathways detected within and across quadrants (Fig. 6C, F, Table 4, Table S8). Metabolite features that had higher concentration in quadrant 1 mapped to tryptophan metabolism, lysine degradation, ubiquinone biosynthesis, and porphyrin metabolism (Fig. 6C, Clusters 2, 6, Table 4, Table S8). Metabolite features that were higher in concentration in quadrant 2 were contained in cluster 1, but no statistically significant pathways were detected. Metabolite features with higher concentrations in quadrant 3 corresponded to mannose type O-glycan biosynthesis and N-glycan biosynthesis (Fig. 6C, Cluster 5, Table 4, Table S8). Metabolite features that had higher concentrations in quadrant 4 mapped to linoleic acid metabolism and primary bile acid biosynthesis (Fig. 6C, Cluster 3, Table 4, Table S8). GAG degradation was detected in quadrants 1 and 3. Alanine, aspartate, and glutamate metabolism was detected in both quadrants 3 and 4 (Table 4, Table S8). Taken together, data suggest spatial location influences, and somewhat reflects, AC metabolism during times of late-stage OA.

[insert Table 4]

Similarly, a median intensity heatmap analysis was performed to identify co-regulated and differentially expressed metabolite features in SB quadrants (Fig. 6F, Table 5, Table S9). Metabolite features that were higher in concentration in quadrant 1 mapped to amino acid metabolism (tyrosine, histidine, phenylalanine, tryptophan, alanine, aspartate, glutamate, valine, leucine, and isoleucine), porphyrin metabolism, glutathione metabolism, retinol metabolism, folate biosynthesis, pyrimidine metabolism, ubiquinone biosynthesis, and GAG biosynthesis (Fig. 6F, Clusters 2, 6, Table 5, Table S9). Metabolite features that were higher in concentration in quadrant 2 mapped to lysine degradation (Fig. 6F, Cluster 5, Table 5, Table S9). Metabolite features higher in concentration in quadrant 3 mapped to fatty acid degradation and phosphatidylinositol signaling (Fig. 6F, Cluster 3, Table 5, Table S9). Metabolite features higher in concentration in quadrant 4 were contained in cluster 1, but no statistically significant pathways were detected. Pathways detected in both quadrants 1 and 3 included purine, arginine, and proline metabolism (Table 5, Table S9). Pathways detected in quadrants 1, 3, and 4 included aminoacyl-tRNA biosynthesis, pantothenate and CoA biosynthesis, and lipid metabolism (glycosphingolipid biosynthesis, GAG degradation, glycerophospholipid metabolism) (Table 5, Table S9). A pathway that was detected across all quadrants was primary bile acid biosynthesis (Table 5, Table S9). Like AC quadrants, SB samples that differ by spatial location exhibit distinct metabolic profiles.

[insert Table 5]

4. DISCUSSION

To the best of our knowledge, this pilot study is the first study to perform global metabolomic profiling to study the OU components AC and SB and their spatial location in late-stage OA samples. The goals of this study were to identify metabolic differences between OU tissues, examine metabolic endotypes associated with grade III and IV OU tissues, and spatially map metabolic differences across regions of AC and SB from OA hip joints. In brief, differences in metabolism between OU components were detected and suggest the osteoarthritic OU components may have different cellular energy requirements. Additionally, different metabolic themes were associated with each OA grade, and pathways like GAG degradation were detected in both OU components and in both grade III and IV samples. Finally, regions of the femoral head that experience peak stress had distinct metabolic endotypes from others. Taken together, this study provides evidence that LC-MS-based global metabolomic profiling can be used to study OA as a whole joint disease, revealing disease-associated metabolic shifts in OU tissues and spatially constrained metabolic shifts associated with disease progression.

4.1 Global metabolomic profiling detects differences between articular cartilage and subchondral bone

Global metabolomic profiling detected differences between OU components. Metabolite features higher in AC were associated with lipid metabolism (glycosphingolipid and arachidonic acid metabolism) and oxidative-phosphorylation (ubiquinone biosynthesis). A previous study conducted by Seito *et al.,* demonstrated the importance of glycosphingolipids in OA development: alterations to chondrocyte-derived glycosphingolipids caused an imbalance in chondrocyte-homeostasis which contributed to the development of OA in transgenic mice[23]. Therefore, the detection of imbalanced glycosphingolipid biosynthesis in AC supports the idea that glycosphingolipids are key regulatory components for AC that negatively influenced tissue health when imbalanced. Arachidonic acid is an unsaturated fatty acid, is associated with prostaglandin synthesis, and has been linked to OA pro-inflammatory responses, suggesting that disease associated metabolic shifts in AC are associated with prostaglandin generation for regulation of inflammation[24-26]. However, previous studies have primarily focused on this metabolic pathway

in knee synovial fluid (SF) and its influence on joint lubrication and inflammation[26-28]. Thus, additional research is required to underpin the relationship between arachidonic acid metabolism at the hip joint and in other joints effected by OA.

Ubiquinones are electron carriers involved in oxidative phosphorylation; therefore, the detection of this pathway may suggest late-stage osteoarthritic AC requires higher ATP demand to support, or rebuild, degrading tissues but further investigation is required to underpin ATP demand during late-stage OA. Lastly, porphyrin metabolism is related to the production of heme, which is paramount to many biological processes. In a previous study, porphyrin was detected in high abundances in SF obtained from end-stage OA patients[29]. The detection of this pathway in diseased SF and AC in the present study, it is possible that this pathway is more dysregulated as OA progresses and metabolites in this pathway are secreted into the SF. However, further investigation is required to better understand the relationship between porphyrin metabolism, AC, and OA disease progression.

Metabolite features higher in SB were associated with amino acid metabolism (alanine, aspartate, glutamate, valine, leucine, and isoleucine metabolism), nucleotide-related pathways (pyrimidine metabolism and aminoacyl-tRNA biosynthesis), and energy pathways (TCA cycle). Nucleotide-related pathways are important for DNA and amino acid synthesis[30]. Amino acids are the building blocks of proteins which are necessary structural elements of the bone extracellular matrix. Because osteophytes often form during late-stage OA, the detection of increased levels of amino acids and nucleotide-related pathways may reflect increased protein synthesis to support bone remodeling and subsequent osteophyte formation. An additional function of amino acids is to enter the TCA cycle to generate ATP. This may suggest that SB utilizes amino acids to generate ATP to help combat the breakdown and wear and tear of late-stage OA. A single study previously study also detected amino acid, energy, and nucleotide-related pathways in mouse bone, validating our findings in SB[31]. These findings suggest that osteoarthritic SB may have a higher cellular demand for nucleotides and amino acids for energy generation, protein synthesis, and bone deposition compared to AC. Taken together, detected pathway differences between AC and SB in the present study align with and support previous studies utilizing OA models and tissues. However, while the observed metabolic differences provide insight into OA in AC and SB, these differences cannot solely be attributed to OA disease progression as healthy controls were absent. Thus, observed differences may also reflect differences in physiology between AC and SB. Future work including healthy controls will confirm detected differences and attribute these differences to either physiology or OA disease progression.

4.2 Distinct metabolic endotypes correspond to radiography-confirmed OA grade

Global metabolomic profiling of osteoarthritic grade III and IV AC and SB confirmed that metabolic changes occur during late-stage OA. Metabolite features that had the highest concentration in grade IV AC, compared to grade III AC, mapped to biosynthesis of unsaturated fatty acids, primary bile acid biosynthesis, pyrimidine metabolism, and histidine metabolism. Conversely, metabolite features highest in grade III AC, compared to grade IV AC, mapped to pantothenate CoA biosynthesis and purine metabolism. Those highest in grade III SB compared to grade IV SB mapped to arachidonic acid metabolism, galactose metabolism, and glycosphingolipid biosynthesis. Conversely, metabolite features associated with arachidonic acid metabolism, galactose metabolism, and glycosphingolipid biosynthesis were highest in grade IV SB compared to grade III SB. GAG degradation was a statistically significant pathway that was detected across all groups.

Galactose metabolism was a metabolic pathway that was detected at statistically significant levels in only one group, grade III AC. Galactose is involved in many cellular processes including

intracellular recognition, glycosylation, GAG synthesis, and can be used to derive cellular energy[32,33]. Previous studies have investigated the role of galactose and its potential role in regulating chondrocyte activity and found that ATDC5 chondrogenic cells and chondrocytes cultured with different concentrations of galactose exhibited increased expression of cartilage matrix type II collagen, aggrecan, and extracellular matrix[32]. This may suggest that galactose promotes chondrogenesis, cartilage repair, and potentially regeneration. Thus, perturbations in galactose metabolism in OA AC may be attempting to combat degradation in the cartilage matrix and generate energy for matrix component synthesis due to the limited bioavailability of other energy sources during late-stage OA. A noteworthy pathway detected in grade IV AC samples was unsaturated fatty acid biosynthesis. Mono and polyunsaturated fats have been associated with reduced joint space width (JSW) in humans[34] and increased cartilage degradation in mice[35]. Radiographic confirmation of grade III and IV OA is associated with a measurable reduction in JSW, with these results supporting supports previous findings that fatty acids influence the pathophysiology of OA[17,36-38]. Taken together, it is evident that acute metabolic differences exist between grade III and IV AC, however, further research is required to understand changes in metabolism as disease progresses from early-stage (grade I and II) to late-stage OA.

There is a large gap in knowledge surrounding OA metabolic alterations in SB. In this study, metabolite features involved in pantothenate CoA biosynthesis and purine metabolism exhibited the greatest alterations in grade III SB. Pantothenate CoA biosynthesis is related to vitamin B5 metabolism, functions as an essential cofactor for lipid synthesis, and can aid in controlling inflammation[39,40]. The detection of this pathway may suggest SB is inflamed and/or is aiding in the synthesis of lipids. Metabolite features associated with purine metabolism were higher in grade III SB. Like pyrimidine metabolism, purine metabolism is important for DNA and amino acid synthesis, which may play a role in osteophyte formation in late-stage OA[41,42]. Alternatively, products of purine metabolism (i.e., purine nucleotide adenosine) are key mediators in the purigenic signaling system, which plays an established role in mediating cell proliferation, differentiation, function, and death in chondrocytes and bone cells and has been previously linked to OA[43-48].

Amongst grade IV SB metabolite features, statistically significant pathways detected included pyrimidine and histidine metabolism. Histidine has been previously linked to different types of arthritis (i.e., OA and rheumatoid arthritis). Sitton *et al.,* examined free histidine levels in synovial fluid (SF) and serum in both OA and rheumatoid arthritis patients and found that that free histidine decreases in rheumatoid arthritis patients and increases in OA patients[49]. Although SF nor serum was obtained for histidine concentration analysis in our current study, the detection of dysregulated histidine metabolism in osteoarthritic SB in the present study supports previous findings and suggests an involvement of histidine metabolism in late-stage OA SB. Like grade III and IV AC findings, end-stage OA displays different metabolic perturbations between grade III and IV SB. Future work can generate, compare, and pinpoint metabolic perturbations that change overtime as disease progresses.

A statistically significant metabolic pathway detected in all four groups was GAG degradation. A known hallmark of OA is a loss of GAG chains of proteoglycans, leading to cartilage degradation[50,51]. Measuring levels of GAGs helps gauge chondrocyte and overall cartilage health. Previous studies have studied GAG loss during OA progression by measuring GAG concentration in SF. Kulkarni *et al*., obtained grade I-IV SF from OA patients and measured GAG concentration using spectrophotometric dye binding assays and found that GAG concentration increased as OA grade increased, reflecting greater cartilage degradation[52]. These previous findings and the detection of altered GAG degradation in osteoarthritic AC in the study herein

support the paradigm that GAGs are a key component of cartilage, reflect chondrocyte health, and are negatively influenced during disease.

GAGs are also a key component of bone where they monitor the activity of osteoclastic and osteogenic factors, regulate the bioavailability of these factors, are a key structural component of the extracellular matrix, and influence bone remodeling[53]. Mansouri *et al.,* investigated GAGs and their role in bone remodeling by studying a specific proteoglycan, syndecan-2, and associated GAGs using a transgenic mouse model. Overexpression of syndecan-2 increased bone surface and mass because resorption was inhibited, increased bone marrow cell apoptosis, and decreased osteoblast and osteoclast precursor populations. These data suggest that GAGs may act as novel facilitators of crosstalk between bone remodeling cells. Considering the work of Mansouri *et al.,* and the detection of GAG degradation in this study, it is likely that underlying SB remodeling is impacted during late-stage OA. To our knowledge no study to date has assessed changes in metabolism across all grades of OA, therefore, generating metabolic profiles of all grades, as well as healthy tissues, could improve current understanding of GAG degradation and general metabolic changes relating to disease progression over time.

4.3 Metabolism reflects spatial location of osteochondral unit components

It is well established that moderate mechanical loading is necessary for joint tissue homeostasis[54-56] and that superior regions of the femoral head experience the greatest stress[11-14]. However, it remains unknown if crosstalk between OA OU components and metabolic disturbances across the joint are influenced by spatial location. To determine it metabolic shifts were spatially constrained to specific regions of the joint, AC and SB samples were taken from four quadrant locations (Fig. 1A-C). We found that metabolic shifts were not uniform across the joint, with variations in metabolic pathway perturbations in each quadrant. Previous evidence has identified superior regions of the femoral head to experience peak stress during physiological loading, which corresponds to quadrants 1 and 3 (Fig. 1A-C). In this study, metabolite features from quadrants that correspond to superior regions experiencing higher mechanical loads mapped to amino acid metabolism (alanine, aspartate, glutamate, lysine), porphyrin metabolism, and GAG degradation. The detection of amino acid metabolism in quadrants that experience peak stress may suggest that amino acids are utilized for energy-generation purposes and protein synthesis to maintain the structural integrity of the extracellular matrix. Given that GAG degradation is an established hallmark of OA, superior quadrants that experience the greatest stress also had the greatest evidence of metabolic alterations consistent with OA. Overall, the detection of metabolic metabolite features and pathways associated with end-stage OA, such as GAG degradation, in regions that experience peak stress may lead to drug targets and improved treatments that are localized to specific regions of the joint to slow, or prevent, disease progression.

4.4 Limitations

This study is not without limitations. Firstly, the number of participants (n=9), and samples (n=65), used for this study is small. Secondly, incomplete participant information was provided (i.e., weight, age, sex) and radiographic scans were unable to be accessed to support OA grade assignment. Thirdly, there were uneven ratios of male to female participants and grade III to grade IV samples. Finally, the lack of healthy, grade I, and II OU tissues limit analyses and therefore limits conclusions.

4.5 Conclusions

To our knowledge, this is the first study to examine OU component metabolism in late-stage osteoarthritis AC and SB. Our data demonstrate that differences in metabolism exist when comparing tissue components, metabolic endotypes reflect OA grade, and that metabolic

perturbations experienced by the joint during late-stage disease are not uniform across the joint. Numerous statistically significant pathways were detected including energy and nucleotide-related pathways and those related to OU tissue homeostasis. It was evident that GAG homeostasis in OU components is negatively influenced during late-stage OA, as well as other metabolic pathways. Furthermore, these data support the notion that OA is a whole-joint disease, and that OU components, and their spatial location, should be examined to best address cartilage-bone crosstalk during disease and late-stage OA. By doing so, potential targets to slow, halt, or reverse disease progression in localized regions of the joint may be identified to overall reduce the physical and economic burdens of OA. Expansion of this study may identify the role of the OU during each stage of disease progression to improve the current understanding of OA pathogenesis.

Abbreviations

OA = osteoarthritis; OU = osteochondral unit; AC = articular cartilage; SB = subchondral bone; LC-MS = liquid chromatography-mass spectrometry, HCA = hierarchical clustering analysis; PCA = principal component analysis; PLS-DA = partial least squares-discriminant analysis; FDR = false discovery rate; GAG = glycosaminoglycan

Acknowledgements

We thank the Mass Spectrometry Facility at Montana State University including Dr. Donald Smith and Jesse Thomas for assisting in LC-MS analysis.

Funding Information

Funding for the Mass Spectrometry Facility used in this publication was made possible by the M.J. Murdock Charitable Trust, the National Institute of General Medical Sciences of the National Institutes of Health (P20GM103474 and S10OD28650), and the MSU Office of Research and Economic Development. This study was funded by the M.J. Murdock Charitable Trust under Award Numbers FSU-2017207 and NS-202016444 (AKH), the National Aeronautics and Space Administration under Award Number 80NSSC20M0042 (AKH), the National Science Foundation under Award Number CMMI 1554708 (RKJ), and the National Institutes of Health under Award Numbers R01AR073964 (RKJ).

Author Contributions

Hope Welhaven: Conceptualization, Data Curation, Formal Analysis, Investigation, Methodology, Resources, Visualization, Writing – original draft, review, and editing. Ethan Viles: Conceptualization, Methodology, Investigation, Data Curation Writing – review and editing. Jenna Starke: Conceptualization, Methodology, Investigation, Writing – review and editing. Cameron Wallace: Methodology, Investigation, Resources, Writing – review and editing. Brian Bothner: Methodology, Resources, Visualization, Validation, Writing – review and editing. Ronald June: Conceptualization, Methodology, Resources, Visualization, Validation, Writing – review and editing, Supervision, Project Administration, Funding Acquisition. Alyssa Hahn: Conceptualization, Methodology, Resources, Visualization, Validation, Writing – review and editing, Supervision, Project Administration, Funding Acquisition.

REFERENCES

[1] M. Cross, E. Smith, D. Hoy, S. Nolte, I. Ackerman, M. Fransen, L. Bridgett, S. Williams, F. Guillemin, C.L. Hill, L.L. Laslett, G. Jones, F. Cicuttini, R. Osborne, T. Vos, R. Buchbinder, A. Woolf, L. March, The global burden of hip and knee osteoarthritis: estimates from the global burden of disease 2010 study, Ann Rheum Dis 73 (2014) 1323-1330. 10.1136/annrheumdis-2013-204763.

[2] D.T. Felson, R.C. Lawrence, P.A. Dieppe, R. Hirsch, C.G. Helmick, J.M. Jordan, R.S. Kington, N.E. Lane, M.C. Nevitt, Y. Zhang, M. Sowers, T. McAlindon, T.D. Spector, A.R. Poole, S.Z. Yanovski, G. Ateshian, L. Sharma, J.A. Buckwalter, K.D. Brandt, J.F. Fries, Osteoarthritis: new insights. Part 1: the disease and its risk factors, Ann Intern Med 133 (2000) 635-646. 10.7326/0003-4819-133-8-200010170-00016.

[3] B. Heidari, Knee osteoarthritis prevalence, risk factors, pathogenesis and features: Part I, Caspian J Intern Med 2 (2011) 205-212.

[4] E.R. Vina, C.K. Kwoh, Epidemiology of osteoarthritis: literature update, Curr Opin Rheumatol 30 (2018) 160-167. 10.1097/BOR.0000000000000479.

[5] E.J. Blain, Involvement of the cytoskeletal elements in articular cartilage homeostasis and pathology, Int J Exp Pathol 90 (2009) 1-15. 10.1111/j.1365-2613.2008.00625.x.

[6] A.E. Peters, R. Akhtar, E.J. Comerford, K.T. Bates, The effect of ageing and osteoarthritis on the mechanical properties of cartilage and bone in the human knee joint, Sci Rep 8 (2018) 5931. 10.1038/s41598-018-24258-6.

[7] R.F. Loeser, S.R. Goldring, C.R. Scanzello, M.B. Goldring, Osteoarthritis: a disease of the joint as an organ, Arthritis Rheum 64 (2012) 1697-1707. 10.1002/art.34453.

[8] M.C. Jewett, G. Hofmann, J. Nielsen, Fungal metabolite analysis in genomics and phenomics, Curr Opin Biotechnol 17 (2006) 191-197. 10.1016/j.copbio.2006.02.001.

[9] Z. Xu, T. Chen, J. Luo, S. Ding, S. Gao, J. Zhang, Cartilaginous Metabolomic Study Reveals Potential Mechanisms of Osteophyte Formation in Osteoarthritis, J Proteome Res 16 (2017) 1425-1435. 10.1021/acs.jproteome.6b00676.

[10] G. Yang, H. Zhang, T. Chen, W. Zhu, S. Ding, K. Xu, Z. Xu, Y. Guo, J. Zhang, Metabolic analysis of osteoarthritis subchondral bone based on UPLC/Q-TOF-MS, Anal Bioanal Chem 408 (2016) 4275-4286. 10.1007/s00216-016-9524-x.

[11] M.D. Harris, A.E. Anderson, C.R. Henak, B.J. Ellis, C.L. Peters, J.A. Weiss, Finite element prediction of cartilage contact stresses in normal human hips, J Orthop Res 30 (2012) 1133-1139. 10.1002/jor.22040.

[12] C.R. Henak, G.A. Ateshian, J.A. Weiss, Finite element prediction of transchondral stress and strain in the human hip, J Biomech Eng 136 (2014) 021021. 10.1115/1.4026101.

[13] B. Xiong, P. Yang, T. Lin, J. Xu, Y. Xie, Y. Guo, C. Liu, Q. Zhou, Q. Lai, W. He, Q. Wei, Q. Zhang, Changes in hip joint contact stress during a gait cycle based on the individualized modeling method of "gait-musculoskeletal system-finite element", J Orthop Surg Res 17 (2022) 267. 10.1186/s13018-022-03094-5.

[14] Z. Zhang, D. Sui, H. Qin, H. Li, Z. Zhang, Contact pressure distribution of the hip joint during closed reduction of developmental dysplasia of the hip: a patient-specific finite element analysis, BMC Musculoskelet Disord 21 (2020) 600. 10.1186/s12891-020-03602-w.

[15] W.C. Bae, M.M. Payanal, A.C. Chen, N.D. Hsieh-Bonassera, B.L. Ballard, M.K. Lotz, R.D. Coutts, W.D. Bugbee, R.L. Sah, Topographic Patterns of Cartilage Lesions in Knee Osteoarthritis, Cartilage 1 (2010) 10-19. 10.1177/1947603509354991.

[16] B.S. Bentley, R.V. Hill, Assessing macroscopic and microscopic indicators of osteoarthritis in the distal interphalangeal joints: a cadaveric study, Clin Anat 20 (2007) 799-807. 10.1002/ca.20511.

[17] J.H. Kellgren, J.S. Lawrence, Radiological assessment of osteo-arthrosis, Ann Rheum Dis 16 (1957) 494-502. 10.1136/ard.16.4.494.

[18] D. Hayashi, F.W. Roemer, A. Guermazi, Imaging for osteoarthritis, Ann Phys Rehabil Med 59 (2016) 161-169. 10.1016/j.rehab.2015.12.003.
[19] A.K. Carlson, R.A. Rawle, E. Adams, M.C. Greenwood, B. Bothner, R.K. June, Application of global metabolomic profiling of synovial fluid for osteoarthritis biomarkers, Biochem Biophys Res Commun 499 (2018) 182-188. 10.1016/j.bbrc.2018.03.117.
[20] A.A. Jutila, D.L. Zignego, B.K. Hwang, J.K. Hilmer, T. Hamerly, C.A. Minor, S.T. Walk, R.K. June, Candidate mediators of chondrocyte mechanotransduction via targeted and untargeted metabolomic measurements, Arch Biochem Biophys 545 (2014) 116-123. 10.1016/j.abb.2014.01.011.
[21] H.D. Welhaven, C.N. McCutchen, R.K. June, Effects of mechanical stimulation on metabolomic profiles of SW1353 chondrocytes: shear and compression, Biol Open 11 (2022). 10.1242/bio.058895.
[22] J. Xia, D.S. Wishart, Using MetaboAnalyst 3.0 for Comprehensive Metabolomics Data Analysis, Curr Protoc Bioinformatics 55 (2016) 14 10 11-14 10 91. 10.1002/cpbi.11.
[23] N. Seito, T. Yamashita, Y. Tsukuda, Y. Matsui, A. Urita, T. Onodera, T. Mizutani, H. Haga, N. Fujitani, Y. Shinohara, A. Minami, N. Iwasaki, Interruption of glycosphingolipid synthesis enhances osteoarthritis development in mice, Arthritis Rheum 64 (2012) 2579-2588. 10.1002/art.34463.
[24] D. Bar-Or, L.T. Rael, G.W. Thomas, E.N. Brody, Inflammatory Pathways in Knee Osteoarthritis: Potential Targets for Treatment, Curr Rheumatol Rev 11 (2015) 50-58. 10.2174/1573397111666150522094131.
[25] D.W. Gilroy, J. Newson, P. Sawmynaden, D.A. Willoughby, J.D. Croxtall, A novel role for phospholipase A2 isoforms in the checkpoint control of acute inflammation, FASEB J 18 (2004) 489-498. 10.1096/fj.03-0837com.
[26] A. Van de Vyver, S. Clockaerts, C.H.A. van de Lest, W. Wei, J. Verhaar, G. Van Osch, Y.M. Bastiaansen-Jenniskens, Synovial Fluid Fatty Acid Profiles Differ between Osteoarthritis and Healthy Patients, Cartilage 11 (2020) 473-478. 10.1177/1947603518798891.
[27] A.M. Mustonen, P. Nieminen, Fatty Acids and Oxylipins in Osteoarthritis and Rheumatoid Arthritis-a Complex Field with Significant Potential for Future Treatments, Curr Rheumatol Rep 23 (2021) 41. 10.1007/s11926-021-01007-9.
[28] P. Nieminen, W. Hamalainen, J. Savinainen, M. Lehtonen, S. Lehtiniemi, J. Rinta-Paavola, P. Lehenkari, T. Kaariainen, A. Joukainen, H. Kroger, T. Paakkonen, A.M. Mustonen, Metabolomics of Synovial Fluid and Infrapatellar Fat Pad in Patients with Osteoarthritis or Rheumatoid Arthritis, Inflammation 45 (2022) 1101-1117. 10.1007/s10753-021-01604-x.
[29] A.K. Carlson, R.A. Rawle, C.W. Wallace, E.G. Brooks, E. Adams, M.C. Greenwood, M. Olmer, M.K. Lotz, B. Bothner, R.K. June, Characterization of synovial fluid metabolomic phenotypes of cartilage morphological changes associated with osteoarthritis, Osteoarthritis Cartilage 27 (2019) 1174-1184. 10.1016/j.joca.2019.04.007.
[30] A. Siddiqui, P. Ceppi, A non-proliferative role of pyrimidine metabolism in cancer, Mol Metab 35 (2020) 100962. 10.1016/j.molmet.2020.02.005.
[31] H.D. Welhaven, Vahidi G et al., The Cortical Bone Metabolome of C57BL/6J Mice Is Sexually Dimorphic, JBMR Plus 6 (2022). 10.1002/jbm4.10654.
[32] Z. Yuan, S. Liu, W. Song, Y. Liu, G. Bi, R. Xie, L. Ren, Galactose Enhances Chondrogenic Differentiation of ATDC5 and Cartilage Matrix Formation by Chondrocytes, Front Mol Biosci 9 (2022) 850778. 10.3389/fmolb.2022.850778.
[33] R.K. June, R. Liu-Bryan, F. Long, T.M. Griffin, Emerging role of metabolic signaling in synovial joint remodeling and osteoarthritis, J Orthop Res 34 (2016) 2048-2058. 10.1002/jor.23420.
[34] B. Lu, J.B. Driban, C. Xu, K.L. Lapane, T.E. McAlindon, C.B. Eaton, Dietary Fat Intake and Radiographic Progression of Knee Osteoarthritis: Data From the Osteoarthritis Initiative, Arthritis Care Res (Hoboken) 69 (2017) 368-375. 10.1002/acr.22952.

[35] C.L. Wu, D. Jain, J.N. McNeill, D. Little, J.A. Anderson, J.L. Huebner, V.B. Kraus, R.M. Rodriguiz, W.C. Wetsel, F. Guilak, Dietary fatty acid content regulates wound repair and the pathogenesis of osteoarthritis following joint injury, Ann Rheum Dis 74 (2015) 2076-2083. 10.1136/annrheumdis-2014-205601.
[36] G.E. Gold, F. Cicuttini, M.D. Crema, F. Eckstein, A. Guermazi, R. Kijowski, T.M. Link, E. Maheu, J. Martel-Pelletier, C.G. Miller, J.P. Pelletier, C.G. Peterfy, H.G. Potter, F.W. Roemer, D.J. Hunter, OARSI Clinical Trials Recommendations: Hip imaging in clinical trials in osteoarthritis, Osteoarthritis Cartilage 23 (2015) 716-731. 10.1016/j.joca.2015.03.004.
[37] J.N. Katz, K.R. Arant, R.F. Loeser, Diagnosis and Treatment of Hip and Knee Osteoarthritis: A Review, JAMA 325 (2021) 568-578. 10.1001/jama.2020.22171.
[38] M.D. Kohn, A.A. Sassoon, N.D. Fernando, Classifications in Brief: Kellgren-Lawrence Classification of Osteoarthritis, Clin Orthop Relat Res 474 (2016) 1886-1893. 10.1007/s11999-016-4732-4.
[39] A.A. Gheita, T.A. Gheita, S.A. Kenawy, The potential role of B5: A stitch in time and switch in cytokine, Phytother Res 34 (2020) 306-314. 10.1002/ptr.6537.
[40] R. Leonardi, S. Jackowski, Biosynthesis of Pantothenic Acid and Coenzyme A, EcoSal Plus 2 (2007). 10.1128/ecosalplus.3.6.3.4.
[41] F. Di Virgilio, E. Adinolfi, Extracellular purines, purinergic receptors and tumor growth, Oncogene 36 (2017) 293-303. 10.1038/onc.2016.206.
[42] J. Yin, W. Ren, X. Huang, J. Deng, T. Li, Y. Yin, Potential Mechanisms Connecting Purine Metabolism and Cancer Therapy, Front Immunol 9 (2018) 1697. 10.3389/fimmu.2018.01697.
[43] P. Gratal, A. Lamuedra, J.P. Medina, I. Bermejo-Alvarez, R. Largo, G. Herrero-Beaumont, A. Mediero, Purinergic System Signaling in Metainflammation-Associated Osteoarthritis, Front Med (Lausanne) 7 (2020) 506. 10.3389/fmed.2020.00506.
[44] M. Koolpe, D. Pearson, H.P. Benton, Expression of both P1 and P2 purine receptor genes by human articular chondrocytes and profile of ligand-mediated prostaglandin E2 release, Arthritis Rheum 42 (1999) 258-267. 10.1002/1529-0131(199902)42:2<258::AID-ANR7>3.0.CO;2-O.
[45] H. Kumagai, B. Sacktor, C.R. Filburn, Purinergic regulation of cytosolic calcium and phosphoinositide metabolism in rat osteoblast-like osteosarcoma cells, J Bone Miner Res 6 (1991) 697-708. 10.1002/jbmr.5650060707.
[46] R.M. Rumney, N. Wang, A. Agrawal, A. Gartland, Purinergic signalling in bone, Front Endocrinol (Lausanne) 3 (2012) 116. 10.3389/fendo.2012.00116.
[47] C. Schofl, K.S. Cuthbertson, C.A. Walsh, C. Mayne, P. Cobbold, A. von zur Muhlen, R.D. Hesch, J.A. Gallagher, Evidence for P2-purinoceptors on human osteoblast-like cells, J Bone Miner Res 7 (1992) 485-491. 10.1002/jbmr.5650070504.
[48] K. Varani, M. De Mattei, F. Vincenzi, S. Gessi, S. Merighi, A. Pellati, A. Ongaro, A. Caruso, R. Cadossi, P.A. Borea, Characterization of adenosine receptors in bovine chondrocytes and fibroblast-like synoviocytes exposed to low frequency low energy pulsed electromagnetic fields, Osteoarthritis Cartilage 16 (2008) 292-304. 10.1016/j.joca.2007.07.004.
[49] N.G. Sitton, J.S. Dixon, H.A. Bird, V. Wright, Serum and synovial fluid histidine: a comparison in rheumatoid arthritis and osteoarthritis, Rheumatol Int 6 (1986) 251-254. 10.1007/BF00541315.
[50] H.J. Mankin, L. Lippiello, Biochemical and metabolic abnormalities in articular cartilage from osteo-arthritic human hips, J Bone Joint Surg Am 52 (1970) 424-434.
[51] M.A. Pratta, W. Yao, C. Decicco, M.D. Tortorella, R.Q. Liu, R.A. Copeland, R. Magolda, R.C. Newton, J.M. Trzaskos, E.C. Arner, Aggrecan protects cartilage collagen from proteolytic cleavage, J Biol Chem 278 (2003) 45539-45545. 10.1074/jbc.M303737200.
[52] P. Kulkarni, S. Deshpande, S. Koppikar, S. Patil, D. Ingale, A. Harsulkar, Glycosaminoglycan measured from synovial fluid serves as a useful indicator for progression of Osteoarthritis and complements Kellgren-Lawrence Score, BBA Clin 6 (2016) 1-4. 10.1016/j.bbacli.2016.05.002.
[53] R. Mansouri, Y. Jouan, E. Hay, C. Blin-Wakkach, M. Frain, A. Ostertag, C. Le Henaff, C. Marty, V. Geoffroy, P.J. Marie, M. Cohen-Solal, D. Modrowski, Osteoblastic heparan sulfate

glycosaminoglycans control bone remodeling by regulating Wnt signaling and the crosstalk between bone surface and marrow cells, Cell Death Dis 8 (2017) e2902. 10.1038/cddis.2017.287.
[54] F. Guilak, B. Fermor, F.J. Keefe, V.B. Kraus, S.A. Olson, D.S. Pisetsky, L.A. Setton, J.B. Weinberg, The role of biomechanics and inflammation in cartilage injury and repair, Clin Orthop Relat Res (2004) 17-26. 10.1097/01.blo.0000131233.83640.91.
[55] N.J. Murphy, J.P. Eyles, D.J. Hunter, Hip Osteoarthritis: Etiopathogenesis and Implications for Management, Adv Ther 33 (2016) 1921-1946. 10.1007/s12325-016-0409-3.
[56] L.A. Setton, V.C. Mow, F.J. Muller, J.C. Pita, D.S. Howell, Mechanical behavior and biochemical composition of canine knee cartilage following periods of joint disuse and disuse with remobilization, Osteoarthritis Cartilage 5 (1997) 1-16. 10.1016/s1063-4584(97)80027-1.

TABLES

Table 1. Partial patient information from total joint arthroplasty donors. Age = years. Height = inches (in). Weight = kilograms (kg). Side = right (R) or left (L) *Indicates missing patient information.

Patient	Age (years)	Sex	Height (inches)	Weight (kg)	Grade	Side
Patient 1	59	M	68	99.8	IV	R
Patient 2	41	M	73	82	IV	R
Patient 3	*	F	64	98	IV	R
Patient 4	44	M	*	*	IV	L
Patient 5	67	M	79	118	IV	R
Patient 6	79	M	69	78	IV	R
Patient 7	70	M	71	73.8	III	L
Patient 8	70	M	70	*	III	L
Patient 9	69	F	71	*	III	L

Table 2. Metabolic pathways associated with articular cartilage and subchondral bone identified by fold change and volcano plot analyses. All pathways listed have a FDR-corrected significance level < 0.05. Articular cartilage = AC. Subchondral bone = SB.

Tissue	Pathway
AC	Porphyrin metabolism
	Arachidonic acid metabolism
	Glycosphingolipid biosynthesis
	Ubiquinone biosynthesis
SB	Alanine, aspartate and glutamate metabolism
	Valine, leucine and isoleucine degradation
	Pyrimidine metabolism
	Aminoacyl-tRNA biosynthesis
	Citrate cycle (TCA cycle)

730 **Table 3.** A) Unique metabolic pathways associated with individual groups including grade III and IV articular cartilage, and grade III and IV subchondral bone. B) Metabolic pathways detected in more than 1 group. Pathways were identified from fold change, volcano plot, and median metabolite intensity heatmap analyses. All pathways listed have a FDR-corrected significance level < 0.05. Articular cartilage = AC. Subchondral bone = SB. G3 = grade III. G4 = grade IV.

735

A) Pathways detected in 1 group

Group	Pathway
AC G3	N-Glycan biosynthesis
	Tryptophan metabolism
	Pentose phosphate pathway
	Galactose metabolism
AC G4	Biosynthesis of unsaturated fatty acids
	Arachidonic acid metabolism
	Glycosphingolipid biosynthesis
	Phosphatidylinositol signaling system
SB G3	Pantothenate and CoA biosynthesis
	Aminoacyl-tRNA biosynthesis
	Purine metabolism
	Primary bile acid biosynthesis
SB G4	Pyrimidine metabolism
	Histidine metabolism
B) Pathways detected in more than 1 group	
AC G3, AC G4, SB G3, SB G4	Glycosaminoglycan degradation
AC G3, AC G4, SB G4	Ubiquinone biosynthesis
	Porphyrin metabolism
AC G3, AC G4	Lysine degradation
SB G3, SB G4	Citrate cycle (TCA cycle)
	Alanine, aspartate and glutamate metabolism
	Valine, leucine and isoleucine degradation

Table 4. A) Unique metabolic pathways associated with specific quadrants including grade III and IV articular cartilage quadrants 1-4. B) Metabolic pathways that were detected in multiple articular cartilage quadrants. Pathways were identified from clusters of co-regulated metabolites in a median metabolite intensity heatmap analysis and those listed have a FDR-corrected significance level of 0.05. Articular cartilage = AC. Q1-Q4 = Quadrants 1-4.

A) Pathways detected in 1 quadrant

Quadrant	Pathway
AC Q1	Tryptophan metabolism
	Lysine degradation
	Ubiquinone biosynthesis
	Porphyrin metabolism
AC Q3	Mannose type O-glycan biosynthesis
	N-Glycan biosynthesis
AC Q4	alpha-Linolenic acid metabolism
	Primary bile acid biosynthesis
B) Pathways detected in more than 1 quadrant	
AC Q1, AC Q3	Glycosaminoglycan degradation
AC Q3 AC Q4	Alanine, aspartate and glutamate metabolism

Table 5. A) Unique metabolic pathways associated with only one specific quadrant including grade III and IV subchondral bone quadrants 1-4. B) Metabolic pathways that were detected in more than 1 quadrant. Pathways were identified from clusters of co-regulated metabolites in a median metabolite intensity heatmap analysis and those listed have a FDR-corrected significance level of 0.05. Subchondral bone = SB. Q1-Q4 = Quadrants 1-4.

A) Pathways detected in 1 quadrant

Quadrant	Pathway
SB Q1	Glycosaminoglycan biosynthesis
	Tyrosine metabolism
	Folate biosynthesis
	Phenylalanine metabolism
	Retinol metabolism
	Pyrimidine metabolism
	Histidine metabolism
	Glutathione metabolism
	Porphyrin metabolism
	Phenylalanine, tyrosine and tryptophan biosynthesis
	Valine, leucine, and isoleucine metabolism
	Alanine, aspartate and glutamate metabolism
SB Q2	Lysine degradation
SB Q3	Phosphatidylinositol signaling system
	Fatty acid degradation
B) Pathways detected in more than 1 quadrant	
SB Q1, SB Q2, SB Q3, SB Q4	Primary bile acid biosynthesis
SB Q1, SB Q3, SB Q4	Aminoacyl-tRNA biosynthesis
	Pantothenate and CoA biosynthesis
	Glycosphingolipid biosynthesis
	Glycerophospholipid metabolism
	Glycosaminoglycan degradation
	Ubiquinone biosynthesis
SB Q1, SB Q3	Purine metabolism
	Arginine and proline metabolism

FIGURES (Color to be used for ALL figures in print)

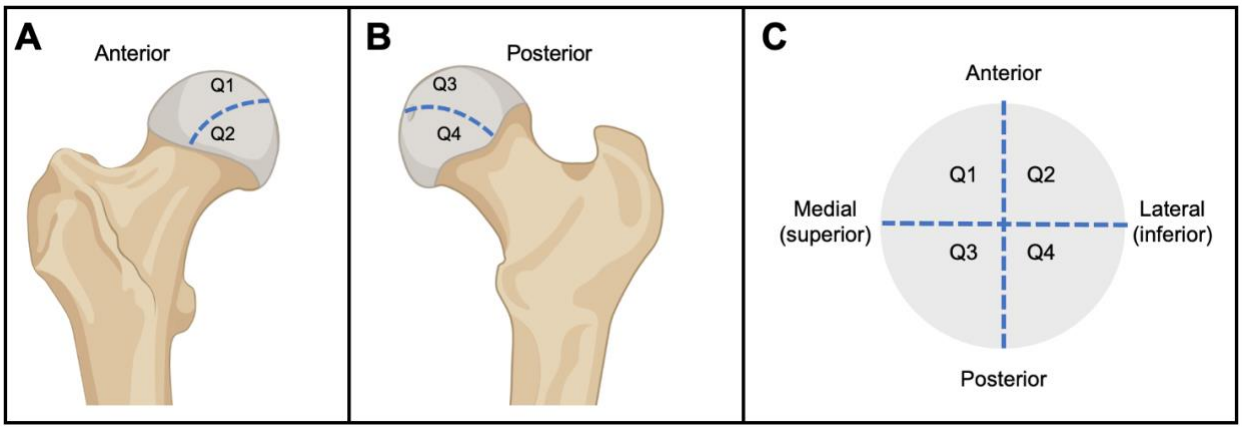

Figure 1. Separation of femoral head into four quadrants based on anatomical position. (A) Anterior and (B) posterior viewing of a right-side femoral head. (C) Quadrants 1 and 2 (Q1-Q2) are anterior superior and inferior quadrants respectively and quadrants 3 and 4 (Q3-Q4) are posterior superior and inferior quadrants, respectively. Both AC and SB were obtained from all four quadrants, therefore, eight possible samples could be obtained per participant.

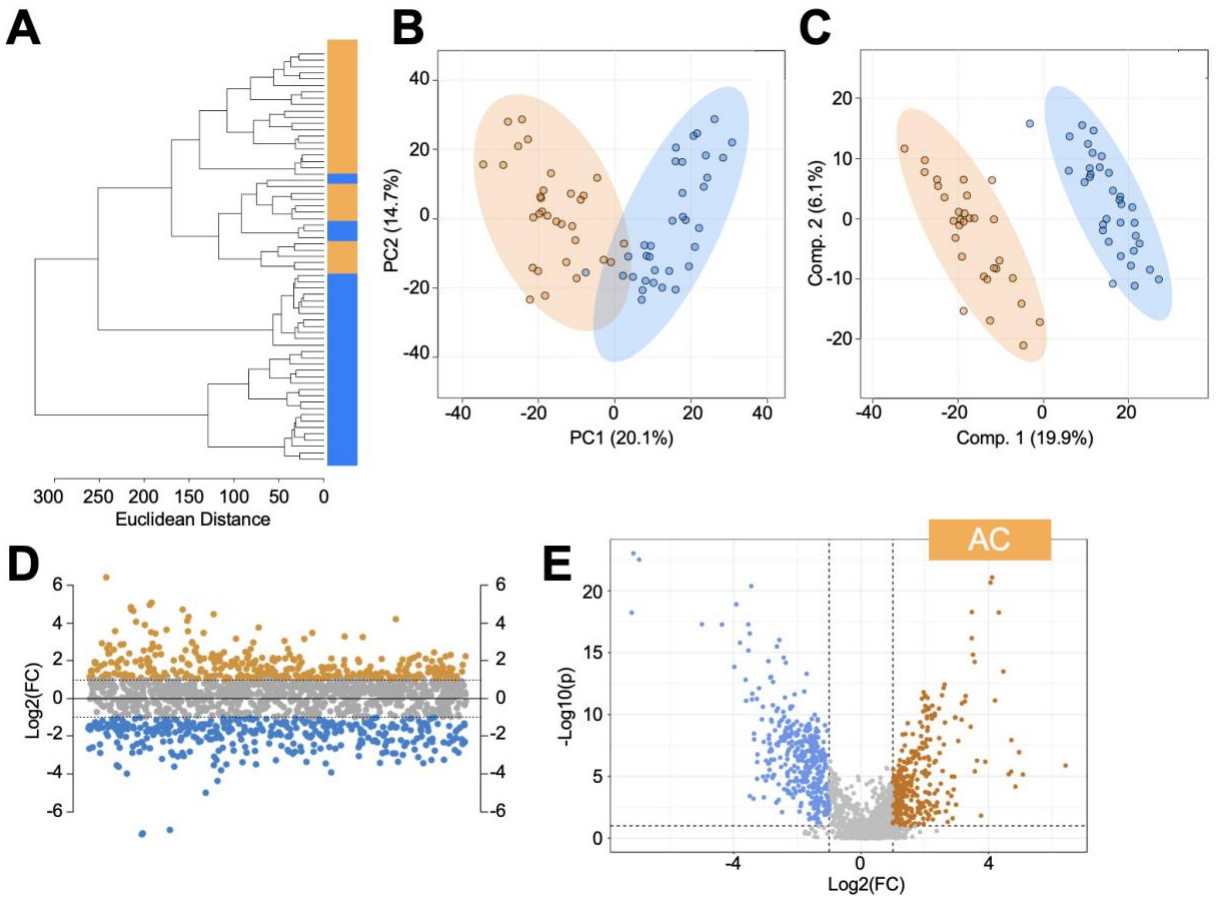

Figure 2. Osteochondral unit components, articular cartilage and subchondral bone, have distinct metabolic endotypes. In total, 1,517 metabolite features were detected across all AC and SB samples (n=31 AC, n=34 SB, n=65 total) and were assessed using multivariate statistical analyses. (A) HCA revealed the metabolomes of each tissue, AC and SB cluster together. (B) PCA visualized overall variation within the dataset and revealed minimal overlap between AC and SB cohorts. Principal components 1 and 2 accounted for 34.8% of the variation of data. (C) PLS-DA showed perfect clustering with no overlap of OU components, with components 1 and 2 accounting for 26% of the variation within the dataset. (D) Fold change analysis identified 360 metabolite features with a FC > 2 that were higher in AC samples compared to SB, whereas 384 metabolite features with a FC < -2 were higher in SB compared to AC. Fold change ratio: AC/SB. (E) Volcano plot analysis identified 318 metabolite features that were higher in AC compared to SB with a FC > 2 and a p-value < 0.05. Conversely, 372 metabolite features that were higher in SB compared to AC had a FC < -2 and a p-value < 0.05. The colors in A-F correspond to osteochondral unit components: orange – articular cartilage (AC), blue – subchondral bone (SB).

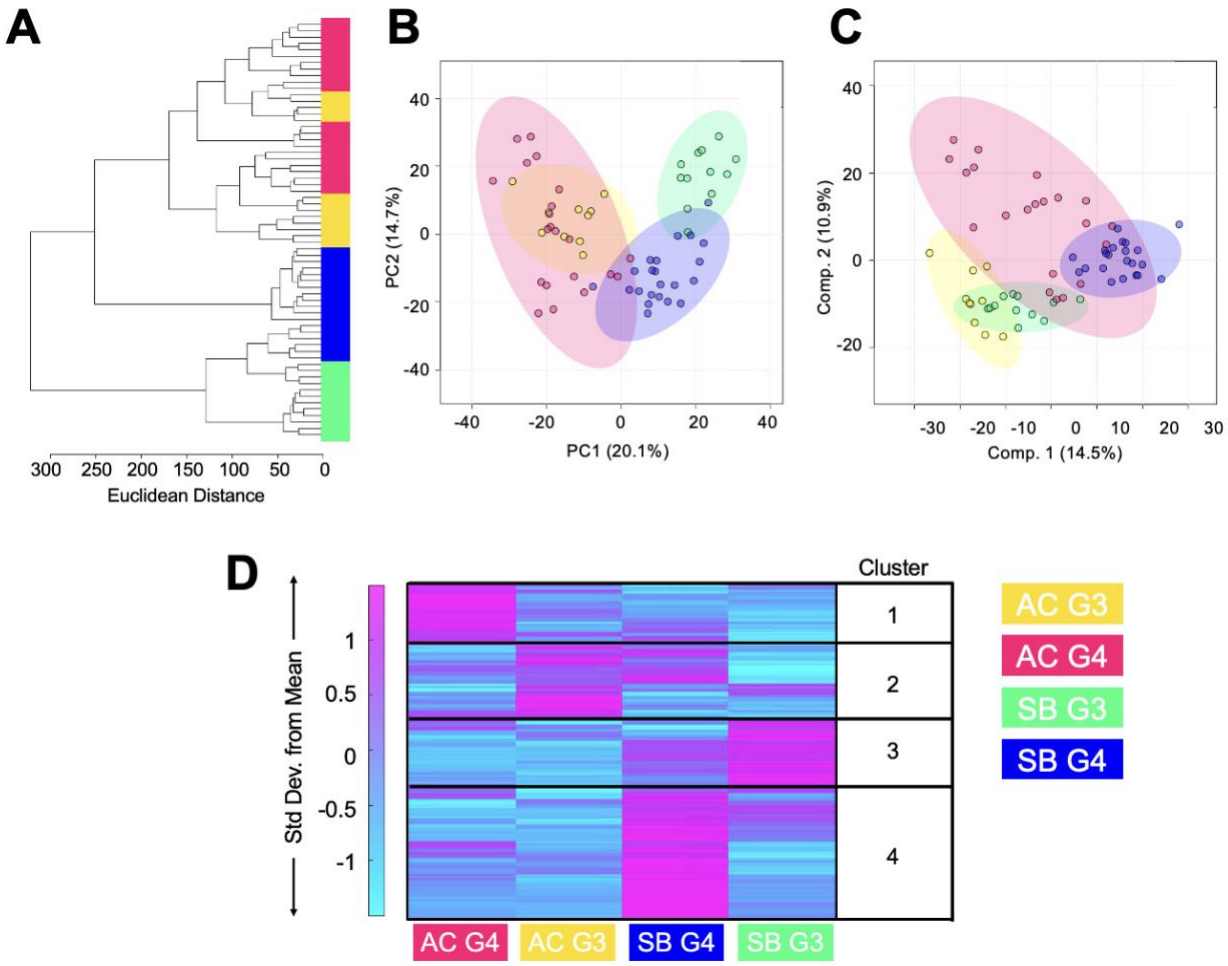
A
300 250 200 150 100 50 0
Euclidean Distance
B
PC2 (14.7%)
PC1 (20.1%)
C
Comp. 2 (10.9%)
Comp. 1 (14.5%)
D
Std Dev. from Mean
1
0.5
0
-0.5
-1
Cluster
1
2
3
4
AC G4
AC G3
SB G4
SB G3
AC G3
AC G4
SB G3
SB G4

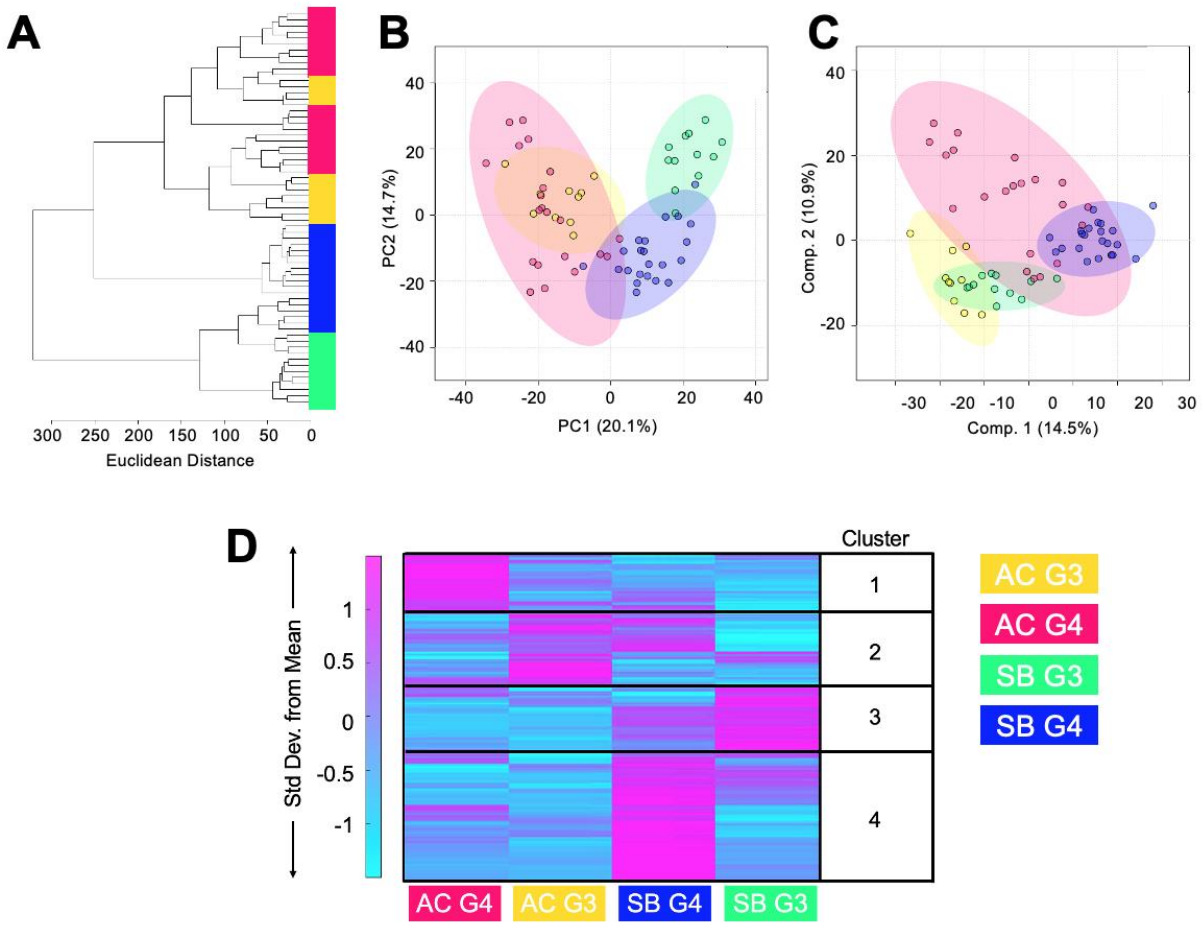

Figure 3. Osteochondral unit component metabolism reflects osteoarthritis grade. (A) HCA displayed that osteochondral unit components (i.e., AC and SB) cluster together, and samples that differ by OA grade (i.e., III, IV) also mostly cluster together. (B) PCA visualized overall variation within the dataset and revealed that the metabolomes of grade III and IV AC and SB are metabolically distinct from each other, with greater metabolic differences exhibited between grade III and grade IV SB as shown my minimal overlap. Principal components 1 and 2 accounted for 34.8% of the variation within the dataset. (C) PLS-DA revealed partial separation between grade III and IV AC and SB where components 1 and 2 accounted for 25.4% of the variation within the dataset. (D) Median metabolite intensity heatmap analysis revealed distinct metabolic endotypes across all groups and clusters of co-regulated metabolites. Clusters of co-regulated metabolites (1-4) outlined in black were selected and mapped to metabolic pathways. The colors in A-D correspond to: articular cartilage grade III – yellow, articular cartilage grade IV – pink, subchondral bone grade III – green, subchondral bone grade IV – blue. Articular cartilage = AC. Subchondral bone = SB.

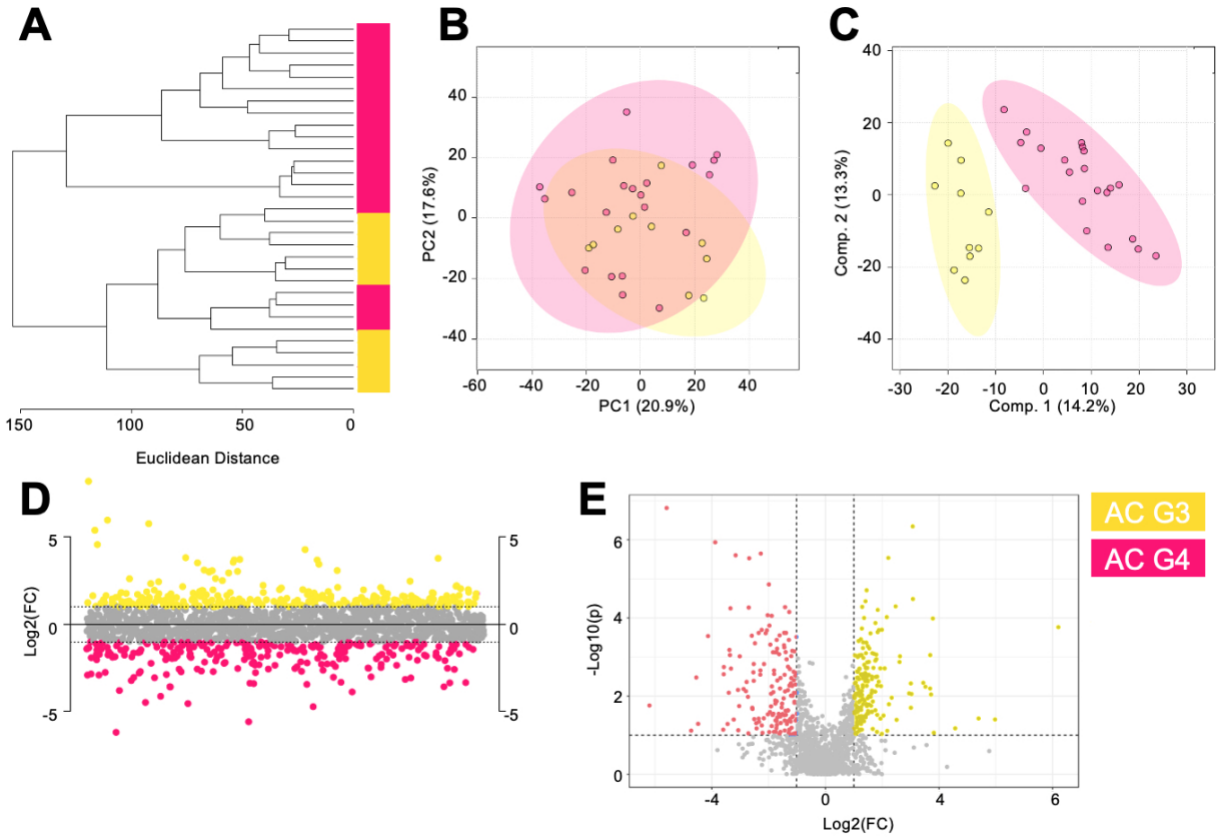

Figure 4. Grade of osteoarthritis influences the metabolome of articular cartilage. (A) HCA showcased that the metabolomes of grade III and IV AC are distinct from one another, as shown by clustering of most samples within their respective cohorts. (B) PCA visualized overall variation within the datasets and found some overlap between AC grades. PC1 and PC2 accounted for 38% of the variation within the dataset. (C) PLS-DA showed clear separation of AC grades. Components 1 and 2 accounted for 27.5% of the variation. (D) Fold change analysis identified 266 metabolite features that were higher in concentration in grade III AC compared to grade IV with a FC > 2, and 259 metabolite features that were higher in concentration in grade IV AC compared to grade III with a FC < -2. Fold change ratio: AC grade III/AC grade IV (E) Volcano plot analysis identified 192 metabolite features higher in grade III AC compared to grade IV that had a FC > 2 and a p-value less than 0.05, whereas 160 metabolite features were higher in grade IV AC compared to grade III that had a FC < -2 and a p-value less than 0.05. The colors in A-F correspond to: grade III articular cartilage - yellow, grade IV articular cartilage – pink. Articular cartilage = AC.

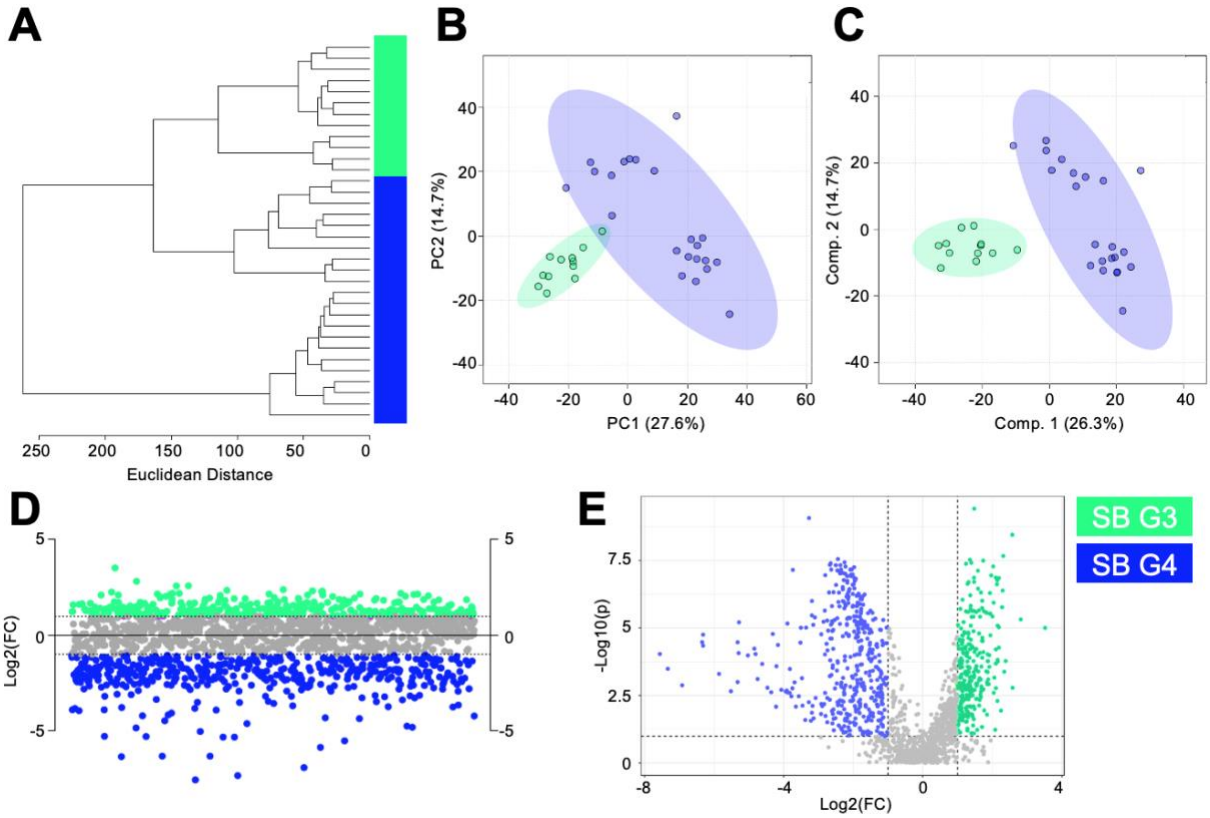

Figure 5. Subchondral bone metabolome reflects osteoarthritis grade. (A) HCA showcased that the metabolomes of grade III and IV SB are distinct from one another, as shown by correct clustering of all samples within their respective cohorts. (B) PCA found minimal overlap between SB grades where PC1 and PC2 accounted for 42.3% of the variation within the dataset. (C) PLS-DA showed clear separation of SB grades, with components 1 and 2 accounting for 41% of the variation within the dataset. (D) Fold change analysis identified 310 metabolite features that were higher in concentration in grade III SB compared to grade IV with a FC > 2 and identified 471 metabolite features that were higher in concentration in grade IV SB compared to grade III with a FC < -2. Fold change ratio: SB grade III/SB grade IV. (E) Volcano plot analysis identified 288 metabolite features higher in grade III SB compared to grade IV that had a FC > 2 and a p-value less than 0.05, whereas 427 metabolite features were higher in grade IV SB compared to grade III that had a FC < -2 and a p-value less than 0.05. The colors in A-F correspond to: grade III subchondral bone – green, grade IV subchondral bone – blue. Subchondral bone = SB.

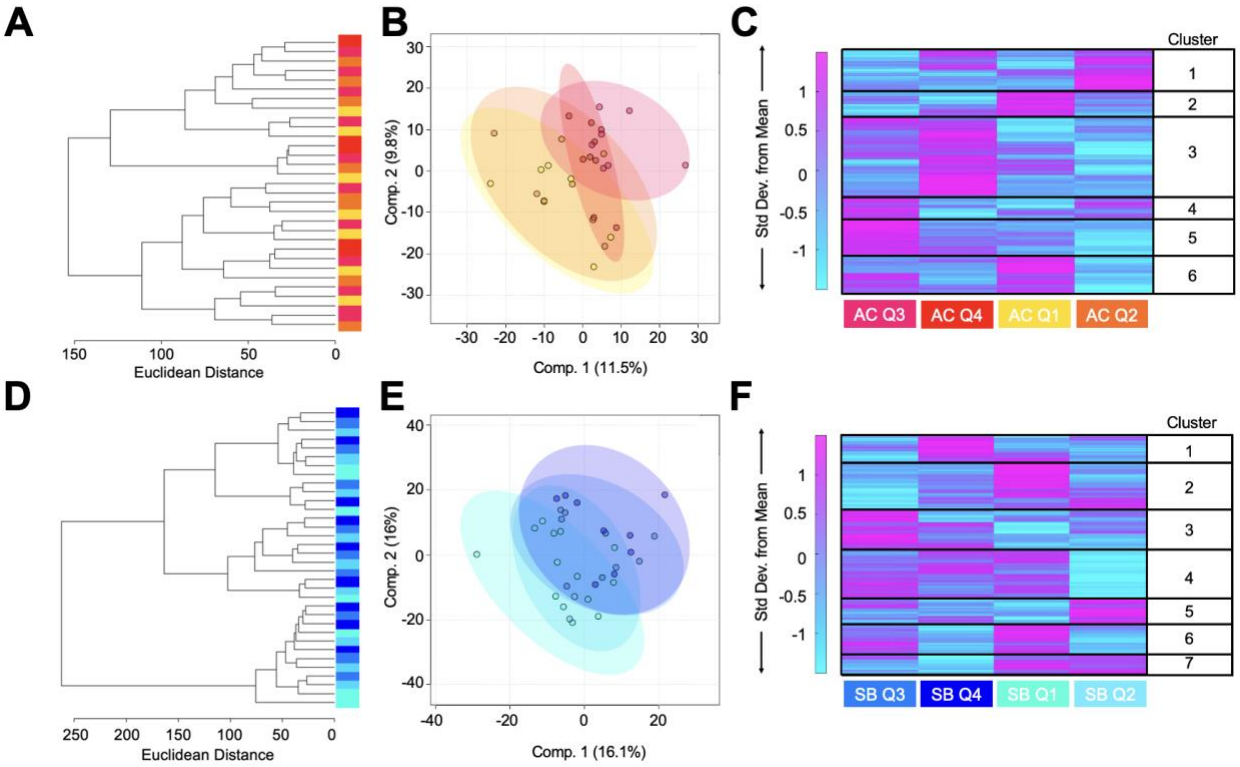

Figure 6. Spatial location of osteochondral unit tissues is reflected in metabolic endotypes. (A) HCA showed minimal separation between AC quadrants. (B) PLS-DA revealed that the metabolome of AC quadrants 1-4 are somewhat metabolically distinct from each other as shown by clustering of samples within respective cohorts although overlap is still evident. (C) Median metabolite intensity heatmap showcased metabolic endotypes by spatial location and identified clusters of co-regulated metabolites. Clusters of co-regulated metabolites (1-6) outlined in black were selected and mapped to metabolic pathways. (D) HCA showcased minimal separation between SB quadrants. (E) PLS-DA revealed clustering of samples within their respective cohorts although overlap is still evident. (F) Median metabolite intensity heatmap showcased metabolic endotypes by spatial location and identified clusters of co-regulated metabolites. Clusters of co-regulated metabolites (1-7) outlined in black were selected and mapped to metabolic pathways. The colors in A-F correspond to: articular cartilage quadrant 1 = yellow, articular cartilage quadrant 2 = orange, articular cartilage quadrant 3 = pink, articular cartilage quadrant 4 = red, subchondral bone quadrant 1 = seafoam green, subchondral bone quadrant 2 = teal, subchondral bone quadrant 3 = light blue, subchondral bone quadrant 4 = dark blue. Articular cartilage = AC. Subchondral bone = SB.

SUPPLEMENTARY FIGURES

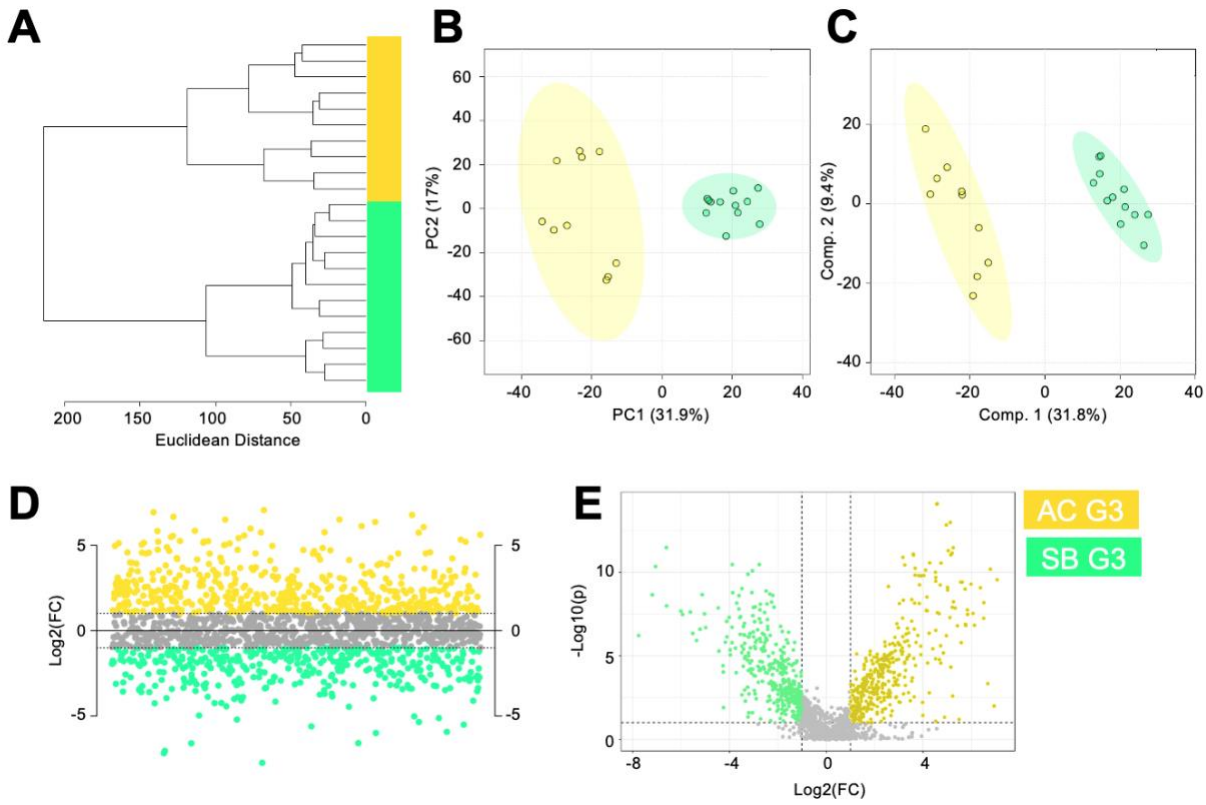

Figure S1. Metabolic differences exist when comparing osteoarthritis grade III articular cartilage and bone. (A) HCA showcased that the metabolomes of grade III SB and AC are distinct from one another, as shown by complete clustering of AC and SB samples within their respective cohorts. (B) PCA found complete separation between grade III SB and AC. PC1 and PC2 accounted for 48.9% of the variation within the dataset. (C) PLS-DA showed clear separation of grade III SB from AC, with components 1 and 2 accounting for 41.2% of the variation within the dataset. (D) Fold change analysis identified metabolite features that were higher or lower in concentration in grade III AC compared to grade III SB (fold change ratio: AC grade III/SB grade III). Fold change analysis identified 501 metabolite features that were higher in concentration in grade III AC compared to SB with a FC > 2. Conversely, fold change analysis identified 392 metabolite features that were higher in concentration in grade III SB compared to grade III AC with a FC < -2. (E) Volcano plot analysis identified 411 metabolite features higher in grade III AC compared to grade III SB that had a FC > 2 and a p-value less than 0.05, whereas 369 metabolite features were higher in grade III SB compared to grade III AC that had a FC < -2 and a p-value less than 0.05. The colors in A-F correspond to: grade III subchondral bone – green, grade III articular cartilage – yellow. Subchondral bone = SB. Articular cartilage = AC.

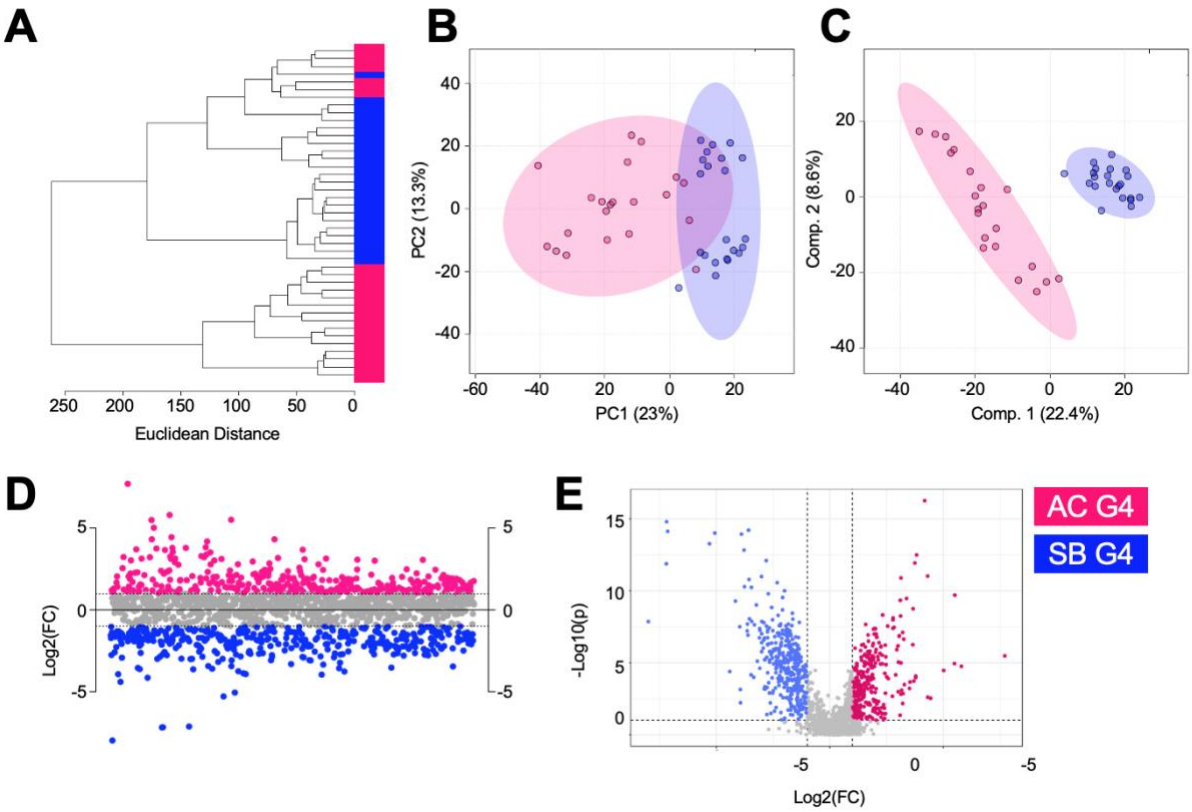

Figure S2. Osteoarthritis grade IV articular cartilage and subchondral bone have distinct metabolic endotypes. (A) HCA showcased that the metabolomes of grade IV SB and AC are distinct from one another, as shown by correct clustering of most AC and SB samples within their respective cohorts. (B) PCA showed separation between grade III SB and AC, with minor overlap. PC1 and PC2 accounted for 36.3% of the variation within the dataset. (C) PLS-DA showed clear separation of grade IV SB from AC, with components 1 and 2 accounting for 31% of the variation. (D) Fold change analysis identified metabolite features that were higher or lower in concentration in grade IV AC compared to grade IV SB (fold change ratio: AC grade IV/SB grade IV. Fold change analysis identified 348 metabolite features that were higher in concentration in grade IV AC compared to SB with a FC > 2. Conversely, fold change analysis identified 400 metabolite features that were higher in concentration in grade IV SB compared to grade IV AC with a FC < -2. (E) Volcano plot analysis identified 291 metabolite features higher in grade IV AC compared to grade IV SB that had a FC > 2 and a p-value less than 0.05, whereas 382 metabolite features were higher in grade IV SB compared to grade IV AC that had a FC < -2 and a p-value less than 0.05. The colors in A-F correspond to: grade IV subchondral bone – blue, grade IV articular cartilage – pink. Subchondral bone = SB. Articular cartilage = AC.

SUPPLEMENTARY TABLES

Table S1. All metabolite features with a fold change > 2 from all pairwise comparisons including articular cartilage and subchondral bone, grades III and IV articular cartilage, grades III and IV subchondral bone, grade III articular cartilage and subchondral bone, and grade IV articular cartilage and subchondral bone.

Table S2. All metabolic pathways outputted from MetaboAnalyst when comparing articular cartilage and subchondral bone using fold change and volcano plot analyses.

Table S3. All metabolic pathways outputted from MetaboAnalyst when comparing grade III and IV articular cartilage and grade III and IV subchondral bone using median metabolite intensity heatmap analysis.

Table S4. All metabolic pathways outputted from MetaboAnalyst when comparing grade III and IV articular cartilage using fold change and volcano plot analyses.

Table S5. All metabolic pathways outputted from MetaboAnalyst when comparing grade III and IV subchondral bone using fold change and volcano plot analyses.

Table S6. All metabolic pathways outputted from MetaboAnalyst when comparing grade III articular cartilage and grade III subchondral bone using fold change and volcano plot analyses.

Table S7. All metabolic pathways outputted from MetaboAnalyst when comparing grade IV articular cartilage and grade IV subchondral bone using fold change and volcano plot analyses.

Table S8. All metabolic pathways outputted from MetaboAnalyst when comparing grade III and IV articular cartilage quadrants 1-4 using median metabolite intensity heatmap analysis.

Table S9. All metabolic pathways outputted from MetaboAnalyst when comparing grade III and IV subchondral bone quadrants 1-4 using median metabolite intensity heatmap analysis.

Supplementary Results

Changes in metabolic profiles correspond to radiography-confirmed grade of OA: Pairwise comparisons

Pairwise comparisons were performed to investigate the metabolomes of samples that differ by tissue and OA grade. First, grade differences within tissue were assessed. HCA of AC grade III vs grade IV samples found that samples clustered within their respective experimental groups (Fig. 4A). PCA showed some overlap between grades, but PLS-DA revealed clear separation of groups (Fig. 4B-C). Fold change analysis identified 266 metabolite features that were expressed in higher concentrations in grade III AC compared to grade IV AC, and 259 metabolite features that were expressed in higher concentrations in grade IV AC compared to grade III AC. Volcano plot analysis identified 192 metabolite features that were significant and had higher concentrations in grade III AC compared to grade IV AC, and 160 metabolite features that were significant and had higher concentrations in grade IV AC compared to grade III AC (Fig. 4E). Next, sub-populations of metabolite features differentially expressed between AC grades identified by fold change and volcano plot analysis underwent pathway enrichment analysis. Metabolite features that were higher in grade III AC compared to grade IV AC mapped to GAG degradation, metabolism of xenobiotics by cytochrome P450, and tryptophan metabolism (Table 3, Table S3). Conversely, metabolite features higher in grade IV AC compared to grade III AC mapped to porphyrin metabolism (Table 3, Table S3).

In a similar way, grade differences within SB samples were studied. HCA displayed clear clustering of grade III and grade IV SB (Fig. 5A). PCA showed minimal overlap of SB samples that differ by grade, whereas PLS-DA displayed clear separation of groups (Fig. 5B-C). To further examine these metabolic differences, fold change and volcano plot analyses were performed. Fold change analysis identified 310 metabolite features that were expressed in higher concentrations in grade III SB compared to grade IV SB, and 371 metabolite features that were

expressed in higher concentrations in grade IV SB compared to grade III SB (Fig. 5D). Next, volcano plot analysis identified 288 metabolite features that were significant and higher in concentration in grade III SB compared to grade IV SB, and 427 metabolite features that were significant and higher in concentration in grade IV SB compared to grade III SB (Fig. 5E). Pathway analyses on the subpopulations identified by these tests revealed both distinct and overlapping pathways between grade III and IV SB. Metabolite features associated with purine metabolism and amino acid metabolism (alanine, aspartate, glutamate) were higher in grade III SB compared to grade IV SB (Table 3, Table S4). Conversely, metabolite features associated with ubiquinone biosynthesis, porphyrin metabolism, and GAG degradation were higher in grade IV SB compared to grade III SB (Table 3, Table S4).

Additionally, tissue differences within the same grade were assessed using the same approach that has been previously described (Fig. S1A-E). When comparing grade III AC and SB, differentially expressed metabolite features identified by fold change and volcano plot analysis underwent pathway enrichment analyses (Fig. S1D-E). Metabolite features higher in grade III SB compared to grade III AC mapped to amino acid metabolism (alanine, aspartate, glutamate, valine, leucine, isoleucine), aminoacyl-tRNA biosynthesis, and phosphatidylinositol signaling system (Table 3, Table S5). Conversely, metabolite features higher in grade III AC compared to grade III SB mapped to steroid hormone biosynthesis, ubiquinone biosynthesis, N-glycan biosynthesis, porphyrin metabolism, and tryptophan metabolism (Table 3, Table S5). GAG degradation was detected in both grade III AC and grade III SB (Table 3, Table S5). The same set of analyses were performed to compare grade IV AC and grade IV SB and differentially expressed metabolite features identified by fold change and volcano plot analyses underwent pathway enrichment analyses (Fig. S2D-E). Metabolite features that were higher in grade IV AC compared to grade IV SB mapped to arachidonic acid metabolism, the pentose phosphate pathway, galactose metabolism, ubiquinone biosynthesis, glycosphingolipid biosynthesis, and lysine degradation (Table 3, Table S6). Conversely, those higher in grade IV SB compared to grade IV AC mapped to amino acid metabolism (alanine, aspartate, glutamate, valine, leucine, isoleucine, histidine), pyrimidine metabolism, and the TCA cycle (Table 3, Table S6). Overall, the results of pathway enrichment analyses of fold change, volcano plot, and median metabolite intensity heatmaps from pairwise and multigroup comparisons strongly suggest that the metabolic endotypes of OU components reflect OA grade (Table 3).